Modeling of Piezoelectric Energy Harvesting from an L-shaped Beam-mass Structure with an Application to UAVs

ALPER ERTURK,[1,*] JAMIL M. RENNO[2] AND DANIEL J. INMAN[2]

[1]*Department of Engineering Science and Mechanics, Center for Intelligent Material Systems and Structures Virginia Tech, Blacksburg, VA 24061, USA*

[2]*Department of Mechanical Engineering, Center for Intelligent Material Systems and Structures, Virginia Tech, Blacksburg, VA 24061, USA*

ABSTRACT: Cantilevered piezoelectric energy harvesters have been extensively investigated in the literature of energy harvesting. As an alternative to conventional cantilevered beams, this article presents the L-shaped beam-mass structure as a new piezoelectric energy harvester configuration. This structure can be tuned to have the first two natural frequencies relatively close to each other, resulting in the possibility of a broader band energy harvesting system. This article describes the important features of the L-shaped piezoelectric energy harvester configuration and develops a linear distributed parameter model for predicting the electromechanically coupled voltage response and displacement response of the harvester structure. After deriving the coupled distributed parameter model, a case study is presented to investigate the electrical power generation performance of the L-shaped energy harvester. A direct application of the L-shaped piezoelectric energy harvester configuration is proposed for use as landing gears in unmanned air vehicle applications and a case study is presented where the results of the L-shaped – energy harvester – landing gear are favorably compared against the published experimental results of a curved beam configuration used for the same purpose.

Key Words: piezoelectricity, energy harvesting, unmanned air vehicles.

INTRODUCTION

VIBRATION-BASED energy harvesting has been investigated by numerous researchers, starting with the early work of Williams and Yates (1996), where the possible vibration-to-electric energy conversion mechanisms were described as piezoelectric, electromagnetic, and electrostatic transductions. These three transduction mechanisms have been studied by researchers extensively in the last decade (Beeby et al., 2006). Theoretical and experimental papers are available on modeling and applications of piezoelectric (Anton and Sodano, 2007), electromagnetic (Arnold, 2007), and electrostatic (Mitcheson et al., 2004) energy harvesters. Among these three alternatives for vibration-to-electric energy conversion, piezoelectric transduction has received the most attention and its literature has already been summarized in three review articles in the last 2 years (Anton and Sodano, 2007; Priya, 2007; Cook-Chennault et al., 2008).

As can be found in the aforementioned review articles, a commonly used piezoelectric energy harvester configuration is a cantilevered beam with one or two piezoceramic layers (a unimorph or a bimorph with the historical definitions, respectively). Typically, the cantilevered energy harvester is located on a vibrating host structure and the dynamic bending strain induced in the piezoceramic layer(s) results in an alternating electric potential difference between the electrodes covering the piezoceramic layer(s). Practical applications (Anton and Sodano, 2007; Priya, 2007; Cook-Chennault et al., 2008) and mathematical modeling (Roundy et al., 2003; Sodano et al., 2004; duToit et al., 2005; Erturk and Inman, 2008a) of cantilevered piezoelectric energy harvesters have been investigated by many researchers in the last 5 years. Practical applications are limited to low-power systems (such as small sensors) (Anton and Sodano, 2007; Priya, 2007; Cook-Chennault et al., 2008) and the respective electromechanical models include single-degree-of-freedom (Roundy et al., 2003; duToit et al., 2005), approximate distributed parameter (Sodano et al., 2004; duToit et al., 2005) and closed-form distributed parameter (Erturk and Inman, 2008a) solutions for predicting the coupled system dynamics

*Author to whom correspondence should be addressed.
E-mail: erturk@vt.edu
Figures 1 and 4–7 appear in color online: http://jim.sagepub.com

1045-389X/09/05 0529–16 $10.00/0 DOI: 10.1177/1045389X08098096

of these piezoelectric energy harvesters. Usually, cantilevered energy harvesters are designed to have a proof mass, which can be tuned to have the fundamental natural frequency of the harvester beam close to a dominant excitation frequency available in the ambient vibration energy spectrum. Although a cantilevered beam is a simple structure that is not very prone to aggressive improvements, the literature includes a considerable effort to improve the electrical outputs of this configuration. Baker et al. (2005) examined the effect of geometry of cantilevered piezoelectric beams on power density to find better alternatives to the rectangular beam shape. Erturk et al. (2008b) discussed how to arrange the electrodes of cantilevered beams and of beams with different boundary conditions to avoid voltage cancellations in energy harvesting. Hu et al. (2007) introduced an axial preload to the conventional cantilevered bimorph configuration to adjust its natural frequency to handle varying-frequency excitations. Hence, the conventional cantilevered beam configuration as a piezoelectric energy harvester has been studied extensively in the literature and a considerable effort has been made to optimize this simple structure for improved electrical outputs.

The aim of this article is to introduce the L-shaped beam-mass structure as a new piezoelectric energy harvester configuration and to analyze its electromechanical behavior. This structure has been investigated in detail in the literature of nonlinear dynamics in the past two decades (Haddow et al., 1984; Balachandran and Nayfeh, 1990) and the relevant nonlinear phenomena observed due to the two-to-one internal resonance (mainly mode saturation) have found interesting applications (Oueini et al., 1998). Here we exploit the unique linear dynamics of the L-shaped structure combined with piezoelectric materials to produce a broader band energy harvester than is available with a simple cantilever configuration. This is followed by a case study presented to analyze the performance of the L-shaped piezoelectric energy harvester. Performance of the harvester as a UAV landing gear is also compared with that of a curved energy harvester beam used for the same purpose in a recent study (Magoteaux, 2007).

FEATURES OF THE L-SHAPED BEAM-MASS STRUCTURE

In this section, some unique features of the L-shaped beam-mass structure are discussed. Although nonlinear modeling is not addressed in this paper, a possible use of the two-to-one internal resonance in energy harvesting is discussed to enhance piezoelectric power generation from base excitation. Then, an advantage of the L-shaped beam-mass structure as a broadband energy harvester is discussed.

Nonlinear Interactions due to Two-to-one Internal Resonance

The L-shaped beam-mass structure has been investigated in the literature of nonlinear dynamics by Haddow et al. (1984) and Balachandran and Nayfeh (1990). As mentioned by Nayfeh and Mook (1979), multi-degree-of-freedom (MDOF) systems having two or more of their natural frequencies commensurable or nearly so (i.e., there exist integers $a_1, \ldots, a_n$ such that $a_1\omega_1 + a_2\omega_2 + \cdots + a_n\omega_n \cong 0$ where $\omega_1, \ldots, \omega_n$ are the natural frequencies) may possess internal resonances. The simplest possible MDOF system is a 2-DOF system and the condition of having $\omega_2 \cong 2\omega_1$ is a simple case for realizing an internal resonance. This particular case is called the two-to-one internal resonance. Although basic structures like cantilevered beams cannot be designed (passively) to obtain $\omega_2 \cong 2\omega_1$, it was shown in the literature (Haddow et al., 1984) that an L-shaped beam-mass structure could have this internal resonance condition (with the third and the higher modes far removed from the first two modes). A structure that has a two-to-one internal resonance and quadratic nonlinearities may exhibit energy exchange between the first two modes, or the so-called saturation phenomenon in case of sinusoidal excitation near a primary resonance (Nayfeh and Mook, 1979). Modal energy exchange is characterized by a continuous back and forth energy exchange between the first two modes. Mode saturation occurs when the excitation amplitude exceeds a certain value, after which the amplitude of the vibration mode that is directly excited becomes independent of the level of excitation and the energy is transferred to the other mode (Nayfeh and Mook, 1979). As a part of our ongoing research, we are investigating the possible use of these unique features of the L-shaped beam-mass structure for piezoelectric energy harvesting. One practical use of nonlinear interactions for piezoelectric energy harvesting is the possibility of obtaining a response at a flexible vibration mode (mode 1) by exciting the harvester at the frequency of a relatively stiff vibration mode (mode 2). That is, the second vibration mode (as the primary resonance) can be directly excited and a voltage response at the first vibration mode can possibly be obtained for large base accelerations due to the saturation phenomenon. This useful scenario is beyond the discussion provided in this article; however, it seems to be realizable owing to the aforementioned previous work on the *passive* L-shaped beam-mass structure. A common criticism of the existing linear

work concerns whether or not the results will be destroyed if the harvester is driven into a nonlinear region at resonance. The saturation phenomenon associated with the L-shaped beam-mass structure and other MDOF systems *with internal resonances* may provide a very useful solution, through the possibility of transferring the input mechanical energy to a more flexible mode and extracting the electrical response at the flexible mode.

L-shaped Beam-mass Structure as a Broadband Energy Harvester

Besides the nonlinear interactions between the vibration modes, the structure is also advantageous as a broadband energy harvester. In most research on piezoelectric energy harvesting, the cantilevered harvester beam has been assumed to be excited at or around its first (fundamental) natural frequency. In other words, the first natural frequency of the harvester is tuned to a frequency that is dominant in the ambient vibration energy. This tuning process is usually realized by means of a proof mass. In reality, however, most ambient vibration sources display random or varying-frequency behavior in time (see, for instance, the random acceleration history of an automobile compressor measured by Sodano et al. (2005) or the sample frequency spectra presented by Roundy et al. (2003)). Hence, in general, ambient vibrations cannot be represented by a single harmonic function. As a consequence, vibration energy available in the ambient excites the higher vibration modes of the harvester structure as well. The nearest vibration mode to the fundamental mode is simply the second mode, and this mode gains importance for random or varying-frequency excitations. Having a vibration mode close to the fundamental vibration mode is preferable for broadband energy harvesting. As far as the conventional cantilevered beam configuration with uniform cross-section is concerned, it is straightforward to show that the second natural frequency is more than 6 times the first natural frequency in the absence of a proof mass ($\omega_2 \cong 6.27\omega_1$). This is simply obtained by taking the ratio of the squares of the dimensionless frequency parameters (eigenvalues) obtained from the respective eigensolution of a clamped-free uniform beam without a proof mass. The presence of a proof mass increases the *relative* spacing of ω_1 and ω_2 of the harvester on the frequency axis even more. Figure 1(a) displays the variation of the dimensionless natural frequencies with dimensionless proof mass-to-beam mass ratio for the first two vibration modes. Taking the ratio of the curves in Figure 1(a) yields ω_2/ω_1, which is a direct measure of the relative spacing between the first two vibration modes on the frequency axis, and the variation of this ratio with proof mass-to-beam mass ratio is plotted in Figure 1(b). As proof mass-to-beam mass ratio ($M_{\text{proof}}/M_{\text{beam}}$) changes from 0 to 10, the ratio between the first two natural frequencies (ω_2/ω_1) increases from 6.27 to 28.7. According to Figure 1(b), the spacing between the first two vibration modes increases monotonically with increasing proof mass and the minimum amount of relative spacing corresponds to the no proof mass case (with $\omega_2 \cong 6.27\omega_1$).

As common practice, the designer tunes the first natural frequency of the harvester beam to a frequency (ω_1) that is dominant in the ambient vibration spectrum. This practice automatically assigns a certain value (ω_2) to the second natural frequency, and we know from Figure 1 that the second natural frequency will not be very close to the first one (at least $\omega_2 \cong 6.27\omega_1$). As a consequence, the response of the harvester to the harmonics in the ambient vibration lying in a very wide frequency range between ω_1 and ω_2 will be considerably weak for random or varying-frequency excitations.

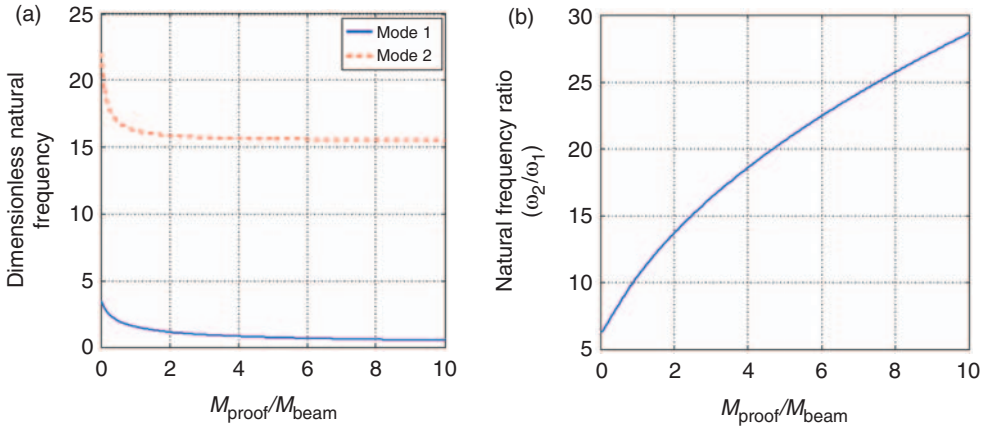

Figure 1. *Variation of the (a) first two dimensionless natural frequencies and (b) their ratio with proof mass-to-beam mass ratio for a conventional uniform cantilevered beam.*

With this consideration, the L-shaped energy harvester configuration proposed in this work has an important advantage over the conventional cantilevered harvesters (with or without a proof mass). While selecting a dominant frequency (ω_1) in the ambient vibration spectrum and setting the first natural frequency of the L-shaped energy harvester to this value, the geometric parameters of the harvester can be tuned to have a second natural frequency (ω_2) that is not very far away from the first natural frequency. For instance, as mentioned before and as will be shown in the case study, $\omega_2 \cong 2\omega_1$ is a realizable case for the L-shaped configuration whereas this case cannot be realized for the conventional cantilevered beams. Thus, it can be concluded that the L-shaped energy harvester configuration has better broadband energy harvester characteristics and is less sensitive to variations in the dominant excitation frequency when compared to the conventional cantilevered beam configuration.

ELECTROMECHANICAL MODELING

In this section, we summarize the electromechanical modeling of the L-shaped unimorph harvester shown in Figure 2(a). The electromechanically coupled modeling approach is based on the experimentally validated (Erturk and Inman, 2008c) coupled distributed parameter model proposed by Erturk and Inman (2008a). As depicted in Figure 2(a), this structure is a combination of one horizontal and one vertical thin beam with two lumped masses (M_1 and M_2). The structure is excited by the vertical base acceleration $a_B(t)$. The substructure and piezoceramic layers are geometrically uniform along their longitudinal directions. The lumped masses and the location of the second lumped mass (M_2) on the vertical beam are important tuning parameters for the system which make it possible to obtain the two-to-one internal resonance for the nonlinear modal interactions mentioned in the previous section.

The vibratory motion of the harvester is examined in three segments (regions), $\Re_k$, equipped with the reference frames (x_k, y_k), such that (Figure 2(b)):

$$\Re_k = \{x_k | 0 \le x_k \le L_k\}, \tag{1}$$

where $k = 1, 2, 3$ in Equation (1) and hereafter. Each segment is modeled for the general case of different lengths L_k, mass per unit length terms m_k, and flexural stiffness terms YI_k. Therefore, the substructure and piezoceramic layers as well as their geometric properties can be taken to be different for each segment $\Re_k$. The piezoceramic layers are covered with conductive electrode pairs and they are poled in the thickness direction (3-direction with the notation of piezoelectricity). The direction of mechanical strain in each segment is the longitudinal direction (1-direction with the notation of piezoelectricity) due to bending deformations. It is assumed that the piezoceramic layer and the substructure layer are perfectly bonded to each other. Segments $\Re_1$, $\Re_2$, and $\Re_3$ have separate electrode pairs whose leads are connected to a single resistive load (R_l) in series. Note that considering a resistive load in the electrical circuit is a common practice in modeling of piezoelectric energy harvesters for persistent vibration inputs. The aim here is to model and investigate the basic electromechanical behavior of the harvester for a resistive electrical load. Circuitry-based discussions with more sophisticated energy harvesting circuit topologies can be found in the literature (e.g., Ottman et al., 2002). Although the configuration is taken as a unimorph in the following analysis, one might as well consider the bimorph case with a similar procedure. The bimorph configuration allows combining the electrical outputs of different segments in series or in parallel, depending on the voltage or current requirements (Erturk and Inman, 2008c).

Modal Analysis for Free Vibrations

Since the aspect ratios of typical energy harvester configurations allow neglect of the effects of shear

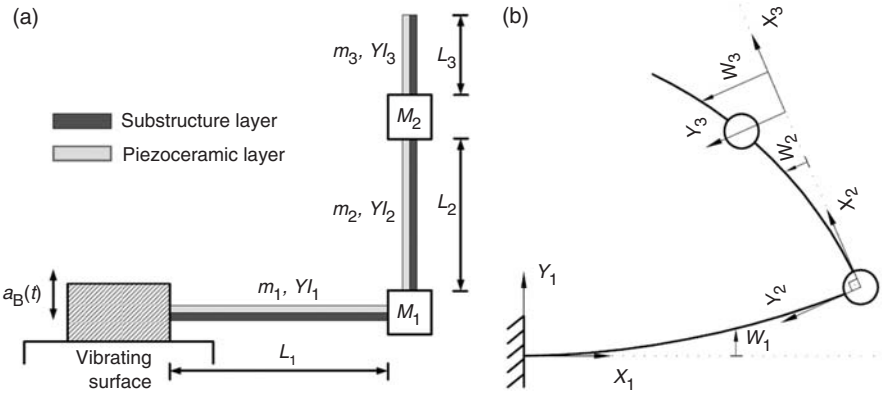

Figure 2. *(a) Schematic of the L-shaped piezoelectric energy harvester, (b) the reference frames and the displacement variables.*

deformation and rotary inertia, the following modeling procedure is based on the Euler-Bernoulli beam assumptions. Reasonably, we are interested in bending vibrations of the harvester and, therefore, the longitudinal vibrations of the beam segments are ignored by assuming the segments to be axially rigid. Geometrically small oscillations are considered here along with the assumption of linearly elastic material behavior. Equations of motion for undamped free vibrations of each segment in its lateral direction can be written as:

$$\frac{\partial^2 (M_b)_k(x_k,t)}{\partial x_k^2} + m_k \frac{\partial^2 w_k(x_k,t)}{\partial t^2} + \delta_{2k} M_2 g \frac{\partial^2 w_k(x_k,t)}{\partial x_k^2} = 0, \quad x_k \in \Re_k, \tag{2}$$

where m_k is the mass per unit length, $(M_b)_k$ (w_k,t) is the bending moment, and $w_k(x_k,t)$ is the transverse vibratory displacement of segment $\Re_k$, M_2 is the second lumped mass (at $x_2 = L_2$), g is the gravitational acceleration, and δ_{rs} is Kronecker delta (defined as being equal to unity for $r = s$ and equal to zero for $r \neq s$). It is important to note that the piezoelectric effect is included in the bending moment $(M_b)_k$ (w_k,t), which can be expanded into a term related to the bending stiffness YI_k and a term related to the voltage $v_k(t)$ across the electrodes of segment $\Re_k$ (Erturk and Inman, 2008a). The expressions of m_k and YI_k for the unimorph cross-section can be found in the Appendix. The dissipative effects due to internal and external damping mechanisms will be introduced as modal damping later. Note that the weight $M_2 g$ of the second lumped mass acts as an axial load for segment $\Re_2$. The boundary conditions, compatibility, and continuity relations are stated next.

The geometric boundary conditions at the clamped end $(x_1 = 0)$ are:

$$w_1(0,t) = 0, \quad \left.\frac{\partial w_1(x_1,t)}{\partial x_1}\right|_{x_1=0} = 0. \tag{3a}$$

The linear/angular displacement and force/moment equilibrium relations at the locations of the lumped masses are:

$$w_2(0,t) = 0, \quad \left.\frac{\partial w_1(x_1,t)}{\partial x_1}\right|_{x_1=L_1} = \left.\frac{\partial w_2(x_2,t)}{\partial x_2}\right|_{x_2=0}, \tag{3b}$$

$$YI_1 \left.\frac{\partial^3 w_1(x_1,t)}{\partial x_1^3}\right|_{x_1=L_1} = (M_1 + M_2 + m_2 L_2 + m_3 L_3) \left.\frac{\partial^2 w_1(x_1,t)}{\partial t^2}\right|_{x_1=L_1}, \tag{3c}$$

$$YI_1 \left.\frac{\partial^2 w_1(x_1,t)}{\partial x_1^2}\right|_{x_1=L_1} + J_1 \left.\frac{\partial^3 w_1(x_1,t)}{\partial t^2 \partial x_1}\right|_{x_1=L_1} = YI_2 \left.\frac{\partial^2 w_2(x_2,t)}{\partial x_2^2}\right|_{x_2=0}, \tag{3d}$$

$$w_2(L_2,t) = w_3(0,t), \quad \left.\frac{\partial w_2(x_2,t)}{\partial x_2}\right|_{x_2=L_2} = \left.\frac{\partial w_3(x_3,t)}{\partial x_3}\right|_{x_3=0}, \tag{3e}$$

$$M_2 g \left.\frac{\partial w_2(x_2,t)}{\partial x_2}\right|_{x_2=L_2} + YI_2 \left.\frac{\partial^3 w_2(x_2,t)}{\partial x_2^3}\right|_{x_2=L_2} = YI_3 \left.\frac{\partial^3 w_3(x_3,t)}{\partial x_3^3}\right|_{x_3=0} + M_2 \left.\frac{\partial^2 w_2(x_2,t)}{\partial t^2}\right|_{x_2=L_2}, \tag{3f}$$

$$YI_2 \left.\frac{\partial^2 w_2(x_2,t)}{\partial x_2^2}\right|_{x_2=L_2} + J_2 \left.\frac{\partial^3 w_2(x_2,t)}{\partial t^2 \partial x_2}\right|_{x_2=L_2} = YI_3 \left.\frac{\partial^2 w_3(x_3,t)}{\partial x_3^2}\right|_{x_3=0}, \tag{3g}$$

where J_1 and J_2 are the rotary inertias of the lumped masses M_1 and M_2, respectively. Finally, the natural boundary conditions at the free end of the harvester can be stated as:

$$YI_3 \left.\frac{\partial^3 w_3(x_3,t)}{\partial x_3^3}\right|_{x_3=L_3} = 0, \quad YI_3 \left.\frac{\partial^2 w_3(x_3,t)}{\partial x_3^2}\right|_{x_3=L_3} = 0. \tag{3h}$$

Based on the expansion theorem, the vibratory motion of beam segment $\Re_k$ can be represented by an absolutely and uniformly convergent series of the eigenfunctions as:

$$w_k(x_k,t) = \sum_{r=1}^{\infty} \phi_{kr}(x_k)\eta_r(t), \quad x_k \in \Re_k, \tag{4}$$

where $\eta_r(t)$ is the modal response of the r-th vibration mode and the piecewise-defined eigenfunctions of the structure are:

$$\phi_{1r}(x_1) = A_{1r}\sin(\alpha_r x_1) + B_{1r}\cos(\alpha_r x_1) + C_{1r}\sinh(\alpha_r x_1) + D_{1r}\cosh(\alpha_r x_1), \tag{5a}$$

$$\phi_{2r}(x_2) = A_{2r}\sin(\beta_r x_2) + B_{2r}\cos(\beta_r x_2) + C_{2r}\sinh(\gamma_r x_2) + D_{2r}\cosh(\gamma_r x_2), \tag{5b}$$

$$\phi_{3r}(x_3) = A_{3r}\sin(\mu_r x_3) + B_{3r}\cos(\mu_r x_3) + C_{3r}\sinh(\mu_r x_3) + D_{3r}\cosh(\mu_r x_3). \tag{5c}$$

The above eigenfunctions are obtained through the separation of variables solution of the respective partial differential equations given by Equation (2).

For harmonic oscillations in time domain, the relations between the frequency parameters of different segments of the structure, natural frequencies, and the structural parameters can be obtained as (Rao, 2007):

$$\alpha_r^4 = \omega_r^2 \frac{m_1}{YI_1}, \quad \mu_r^4 = \omega_r^2 \frac{m_3}{YI_3},$$
$$\beta_r^2 = \frac{\kappa}{2} + \sqrt{\frac{\kappa^2}{4} + \omega_r^2 \frac{m_2}{YI_2}}, \tag{6}$$
$$\gamma_r^2 = -\frac{\kappa}{2} + \sqrt{\frac{\kappa^2}{4} + \omega_r^2 \frac{m_2}{YI_2}}, \quad \kappa = \frac{M_2 g}{YI_2}$$

where ω_r is the undamped natural frequency of the r-th vibration mode. Note that the above modal analysis is given for the short circuit conditions of the system (i.e., $R_l \to 0$, where R_l is the load resistance). The undamped natural frequencies (ω_r) are approximately the short circuit resonance frequencies (ω_r^{sc}) of the system for light mechanical damping (since the voltage feedback in the beam equation tends to zero for $R_l \to 0$). Due to the piezoelectric coupling in the mechanical equation (which is embedded in the bending moment term in Equation (2)), the short circuit resonance frequency ω_r^{sc} of the r-th vibration mode shifts to the open circuit resonance frequency ω_r^{oc} as $R_l \to \infty$. For nonzero and finite values of load resistance, the resonance frequency of the r-th vibration mode takes a value between the short circuit and the open circuit resonance frequencies (Erturk and Inman, 2008a,c).

As a common practice, substituting Equation (4) in Equations (3a)–(3h) results in an eigenvalue problem. Using the differential eigensolution procedure, the resulting 12×12 coefficient matrix is forced to be singular and the natural frequencies of the structure are obtained from the resulting characteristic equation. The natural frequencies are then used in Equations (5a)–(5c) and Equation (6) to find the eigenfunctions of each segment. In Equations (5a)–(5c), $\{A_{kr}, B_{kr}, C_{kr}, D_{kr},\}$ are the modal coefficients of the eigenfunction defined over segment $\Re_k$, respectively. Therefore, the modal contributions of the eigenfunctions in the series expansions depend on these sets of modal coefficients. It is then required to normalize the piecewise-defined (but continuous) eigenfunctions over the entire domain $\Re_1 \cup \Re_2 \cup \Re_3$. In order to be consistent with the formulation proposed by Erturk and Inman (2008a) for a unimorph cantilevered beam, the piecewise-defined eigenfunctions of the structure are *mass normalized* according to the orthogonality condition given by:

$$\sum_{k=1}^{3} \int_0^{L_k} m_k \phi_{kr}(x_k)\phi_{ks}(x_k)\mathrm{d}x_k + (M_1 + M_2 + m_2 L_2 + m_3 L_3)\phi_{1r}(L_1) \times \phi_{1s}(L_1) + M_2 \phi_{2r}(L_2)\phi_{2s}(L_2) + J_1 \frac{\mathrm{d}\phi_{1r}(x_1)}{\mathrm{d}x_1}\bigg|_{x_1=L_1} \frac{\mathrm{d}\phi_{1s}(x_1)}{\mathrm{d}x_1}\bigg|_{x_1=L_1} + J_2 \frac{\mathrm{d}\phi_{2r}(x_2)}{\mathrm{d}x_2}\bigg|_{x_2=L_2} \frac{\mathrm{d}\phi_{2s}(x_2)}{\mathrm{d}x_2}\bigg|_{x_2=L_2} = \delta_{rs}, \tag{7}$$

and its stiffness counterpart (which is automatically satisfied when Equation (7) is satisfied).

Electromechanical Equations for General Base Excitation

In order to derive the electromechanical equations of the harvester, one should first consider the effect of mechanical forcing in the system. Since the base excitation is in the vertical direction in the physical coordinates (which is the y_1-direction in Figure 2(b)), the direct excitation of the structure is due to its own inertia in the same direction. Therefore, as one is interested in bending vibrations of the harvester, it is straightforward to see from Figure 2(b) that the forcing will affect Equation (2) for $k = 1$ in the physical coordinates. However, the entire structure will be vibrating due to the formulation given in the previous section. After substituting Equation (4) into Equation (2) and applying the orthogonality conditions, the forced equation of motion can be written in the modal coordinates as:

$$\frac{\mathrm{d}^2\eta_r(t)}{\mathrm{d}t^2} + 2\zeta_r\omega_r\frac{\mathrm{d}\eta_r(t)}{\mathrm{d}t} + \omega_r^2\eta_r(t) + \sum_{k=1}^{3}\chi_{kr}v_k(t) = N_r(t), \tag{8}$$

where ζ_r is the viscous modal damping ratio of the r-th vibration mode,[1] $v_k(t)$ is the voltage across the electrodes in segment $\Re_k$, χ_{kr} is the modal electromechanical coupling term and $N_r(t)$ is the modal mechanical forcing function such that:

$$\chi_{kr} = \vartheta_k \frac{\mathrm{d}\phi_{kr}(x_k)}{\mathrm{d}x_k}\bigg|_0^{L_k}, \tag{9a}$$

$$N_r(t) = -\Big[m_1 \int_0^{L_1} \phi_{1r}(x_1)\mathrm{d}x_1 + (M_1 + M_2 + m_2 L_2 + m_3 L_3)\phi_{1r}(L_1)\Big] a_B(t). \tag{9b}$$

[1]For a detailed discussion on how to relate the modal damping ratio to the internal (strain rate) and external (air) damping terms based on the proportional damping assumption, the reader is referred to Erturk and Inman (2008a, 2008d).

Here, ϑ_k is the coupling term in the physical coordinates for the piezoceramic layer in $\Re_k$ and it is given in the Appendix. The modal forcing function given by Equation (9b) is due to the lateral inertia of the distributed mass in $\Re_1$ as well as the lumped mass at the boundary $x_1 = L_1$, which includes the masses of the vertical beam segments, and the lumped masses M_1 and M_2. Note that in the modal forcing function the forcing term due to external damping effect is neglected (Erturk and Inman, 2008d).

Figure 3 displays the electrical circuit of the L-shaped energy harvester where the electrical outputs of the piezoceramic layers of segments $\Re_1$, $\Re_2$ and $\Re_3$ are combined series and connected to a resistive load R_l. Each piezoceramic layer is shown as a current source along with its internal (or inherent) capacitance connected in parallel. The electric current $i_k(t)$ produced in each segment $\Re_k$ is given by:

$$i_k(t) = \sum_{r=1}^{\infty} \psi_{kr} \frac{\mathrm{d}\eta_r(t)}{\mathrm{d}t} \tag{10}$$

where:

$$\psi_{kr} = -(\mathrm{d}_{31})_k (Y_p)_k (h_{pc})_k \mathrm{b}_k \frac{\mathrm{d}\phi_{kr}(x_k)}{\mathrm{d}x_k}\bigg|_0^{L_k}. \tag{11}$$

In Equation (11), $(\mathrm{d}_{31})_k$ is the piezoelectric constant, $(Y_p)_k$ is Young's modulus (i.e., elastic stiffness at constant electric field), b_k is the width of the piezoceramic layer and $(h_{pc})_k$ is the distance between the center of the piezoceramic layer and the neutral axis of the unimorph cross-section in $\Re_k$ (see the Appendix). Note that the above form of Equation (10) assumes the electrodes of $\Re_1$, $\Re_2$ and $\Re_3$ to be insulated from each other, i.e., they are discontinuous at $x_1 = L_1$ and $x_2 = L_2$. As can be seen from Equations (10) and (11), the electric current generated in each segment is proportional to the bending slope difference at the electrode boundaries. This is due to the fact that the electric current is the time rate of change of the electric displacement integrated over the electrode area, where the electric displacement is proportional to the curvature of the beam (Erturk and Inman, 2008a, b). Therefore, one should be careful about the mode shapes of the structure when combining the current outputs. Otherwise, depending on the mode shapes, cancellations of the current outputs are possible as demonstrated in the following case study.

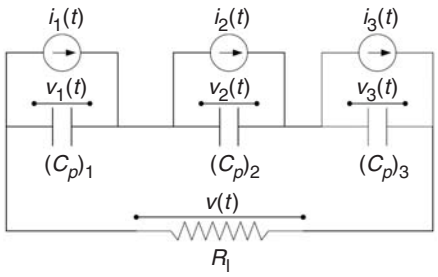

Figure 3. *Electrical circuit of the L-shaped piezoelectric energy harvester (series connection).*

The internal capacitance $(C_p)_k$ of the piezoceramic layer in segment $\Re_k$ can be obtained from:

$$(C_p)_k = \frac{\left(\varepsilon_{33}^S\right)_k b_k L_k}{(h_p)_k}, \tag{12}$$

where $(\varepsilon_{33}^S)_k$ is the permittivity of the piezoceramic layer at constant strain and $(h_p)_k$ is the thickness of the piezoceramic layer. Note that the form of Equation (12) assumes that the entire length of the piezoceramic layer in segment $\Re_k$ is covered with continuous electrodes.

Applying the Kirchhoff Laws to the circuit shown in Figure 3 and employing Equation (10) results in the following three equations for $v_1(t)$, $v_2(t)$ and $v_3(t)$:

$$\frac{1}{R_l} v_1(t) + (C_p)_1 \frac{\mathrm{d}v_1(t)}{\mathrm{d}t} + \frac{1}{R_l} v_2(t) + \frac{1}{R_l} v_3(t) = \sum_{r=1}^{\infty} \psi_{1r} \frac{\mathrm{d}\eta_r(t)}{\mathrm{d}t}, \tag{13a}$$

$$\frac{1}{R_l} v_1(t) + \frac{1}{R_l} v_2(t) + (C_p)_2 \frac{\mathrm{d}v_2(t)}{\mathrm{d}t} + \frac{1}{R_l} v_3(t) = \sum_{r=1}^{\infty} \psi_{2r} \frac{\mathrm{d}\eta_r(t)}{\mathrm{d}t}, \tag{13b}$$

$$\frac{1}{R_l} v_1(t) + \frac{1}{R_l} v_2(t) + \frac{1}{R_l} v_3(t) + (C_p)_3 \frac{\mathrm{d}v_3(t)}{\mathrm{d}t} = \sum_{r=1}^{\infty} \psi_{3r} \frac{\mathrm{d}\eta_r(t)}{\mathrm{d}t}. \tag{13c}$$

Equation (8) and Equations (13a)–(13c) constitute four ordinary differential equations for the four unknowns $v_1(t)$, $v_2(t)$, $v_3(t)$, and $\eta_r(t)$. These equations are the electromechanical equations of the L-shaped energy harvester. The voltage response across the resistive load is simply;

$$v(t) = \sum_{k=1}^{3} v_k(t), \tag{14}$$

and the coupled mechanical response of the harvester in the desired segment can be obtained by using $\eta_r(t)$ in Equation (4) along with the eigenfunctions, which are normalized according to Equation (7).

Coupled Voltage Response and Vibration Response for Harmonic Base Excitation

As is common practice in the energy harvesting literature, we assume the base acceleration to be harmonic of the form $a_B(t) = A_B e^{j\omega t}$ where A_B is the amplitude of the base acceleration, ω is the excitation frequency, and j is the unit imaginary number. For linear oscillations, the steady state expressions for the modal mechanical response $\eta_r(t)$ and the voltage response $v_k(t)$ of the harvester can be written as:

$$\eta_r(t) = H_r e^{j\omega t}, \quad v_k(t) = V_k e^{j\omega t}, \tag{15}$$

respectively, where Hr and V_k are the complex valued amplitudes. Using Equation (8) and Equation (15) results in the following relationship:

$$H_r = \frac{\lambda_r A_B - \sum_{k=1}^{3} \chi_{kr} V_k}{\omega_r^2 - \omega^2 + j2\zeta_r\omega_r\omega}, \tag{16}$$

where

$$\lambda_r = -\Big[m_1 \int_0^{L_1} \phi_{1r}(x_1)\mathrm{d}x_1 + (M_1 + M_2 + m_2 L_2 + m_3 L_3)\phi_{1r}(L_1)\Big]. \tag{17}$$

Eliminating the modal mechanical response term in Equations (13a)–(13c) results in three equations for V_1, V_2, and V_3 which can be written in the contracted notation as:

$$\sum_{k=1}^{3} Q_{mk} V_k = P_m, \quad \text{where } m = 1, 2, 3. \tag{18}$$

Here,

$$Q_{mk} = \frac{1}{R_l} + j\omega(C_p)_m\delta_{mk} + \sum_{r=1}^{\infty} \frac{j\omega\psi_{mr}\chi_{kr}}{\omega_r^2 - \omega^2 + j2\zeta_r\omega_r\omega},$$
$$P_m = \sum_{r=1}^{\infty} \frac{j\omega\psi_{mr}\lambda_r A_B}{\omega_r^2 - \omega^2 + j2\zeta_r\omega_r\omega} \tag{19}$$

are complex valued.

The closed-form solution of the complex voltage amplitude V_k can be obtained from Equation (18), which can be used in Equation (15) to obtain the steady state voltage response expressions across the electrodes of the individual piezoceramic layers. Then, the complex voltage amplitude across the resistive load is:

$$V = \sum_{k=1}^{3} V_k. \tag{20}$$

The complex amplitude of the electric current passing through the resistive load is $I = V/R_l$ and the peak electrical power amplitude is $P = |V|^2/R_l$. Note that V is the peak voltage amplitude and the root mean square value of the voltage is simply $V_{rms} = V/\sqrt{2}$, which yields an average power of $P_{ave} = P/2$.

In order to obtain the coupled vibration response of the harvester, one should use V_1, V_2, and V_3 in H_r (Equation (16)), which can then be used in Equation (15), and eventually in Equation (4) to obtain the coupled physical response of the harvester.

CASE STUDY

In this section, an L-shaped unimorph energy harvester under harmonic base excitation is analyzed. Rather than specifying a certain frequency for the base excitation, the coupled response characteristics of the harvester structure (mechanical and electrical) are investigated with frequency response functions (FRFs). The material, geometric, and electromechanical properties of the harvester are given in Tables 1 and 2. The substructure is made of steel and the material of the piezoceramic layer is PZT-5A. In addition to the numerical data provided in the tables, the structure has two lumped masses $M_1 = 0.025\,\mathrm{kg}$ and $M_1 = 0.015\,\mathrm{kg}$ at $x_1 = L_1$ and $x_2 = L_2$, respectively, and these masses have the rotary inertias $J_1 = 1.5 \times 10^{-6}\,\mathrm{kg/m^2}$ and $J_2 = 1 \times 10^{-6}\,\mathrm{kg/m^2}$, respectively. Although the following is a linear analysis based on the model derived in the previous section, the unimorph harvester of this case study is designed to have $\omega_2 \cong 2\omega_1$ where $\omega_1^{sc} \cong 22.8$ Hz and $\omega_2^{sc} \cong 45.7$ Hz under short circuit conditions (i.e., $R_l \to 0$).[2] It is observed that the first two open circuit natural frequencies of the harvester are $\omega_1^{oc} \cong 23.8$ and $\omega_2^{oc} \cong 46.5$ Hz, respectively, for $R_l \to \infty$. The shift in the natural frequencies with changing load resistance is an expected trend, as previously observed for conventional piezoelectric energy harvesters (Erturk and Inman, 2008a, c). Thus, for finite (and nonzero) values of load resistance, the resonance frequencies of the harvester take values between the short circuit and open circuit resonance frequencies. It is observed from the literature that the resonance frequency of a vibration mode has a value between these two frequencies for more complicated

[2]In order to design the structure with this internal resonance condition in a simple way, a 6-DOF model of the structure (with three translational and three rotational DOFs) is obtained (Chopra, 2007), and then it is reduced to a 2-DOF model by using the static condensation technique (Guyan, 1965).

energy harvesting circuits as well (see, for instance, Lesieutre et al., 2004). This is reasonable since the impedance across the electrodes is limited between these two extreme cases (short circuit and open circuit conditions).

Before discussing the trends in the resulting FRFs, an important issue regarding the mode shape dependence of the electrical outputs must be addressed. It can be recalled from Figure 3 that the individual piezoceramic layers are modeled as current sources in parallel to their internal capacitances. Equation (10) shows that the current source $i_k(t)$ of segment $\Re_k$ is a function of the modal velocity response $d\eta_r(t)/dt$ and the mode shape dependent parameter ψ_{kr}. In case of excitation around a vibration mode ($\omega \cong \omega_r$), the summation in Equation (10) reduces to a single dominating term. Then, from the expression given for ψ_{kr}, the amplitude and phase of the current source depend on the bending slope difference at the electrode boundaries in segment $\Re_k$. To improve the charge collected in segment $\Re_k$, one should make this slope difference as large as possible. Strong cancellations may occur when harvesting energy from a certain vibration mode if continuous electrodes cover a region where the curvature (and therefore the bending strain) changes sign for that vibration mode (Erturk and Inman, 2008a, b).

Table 1. Material and electromechanical properties of the L-shaped unimorph energy harvester.

Property	Substructure	Piezoceramic
Young's modulus (GPa)	200	66
Mass density (kg/m^3)	7800	7800
Piezoelectric constant, d_{31} (pm/V)	–	−190
Permittivity, ε_{33}^S (nF/m)	–	13.27

Table 2. Geometric properties of the L-shaped unimorph energy harvester.

Segment	Dimension	Substructure	Piezoceramic
$\Re_1$	Length (mm)	50	50
	Width (mm)	10	10
	Thickness (mm)	0.5	0.5
$\Re_2$	Length (mm)	39.6	39.6
	Width (mm)	8	8
	Thickness (mm)	0.3	0.3
$\Re_3$	Length (mm)	20.4	20.4
	Width (mm)	8	8
	Thickness (mm)	0.3	0.3

Figure 4(a) and (b) display the piecewise-defined mode shapes of the L-shaped energy harvester for modes 1 and 2, respectively. It is clear from Figure 4(a) that the slope difference in all three segments has the same sign for mode 1 excitations. Consequently, the current source terms $i_1(t)$, $i_2(t)$, and $i_3(t)$ of segments $\Re_1$, $\Re_2$, and $\Re_3$ in Figure 3 are in-phase and they do not cancel one another for direct combination of the electrode leads in mode 1 excitation. However, as can be seen from Figure 4(b), this is not the case for the second mode shape, since the slope difference at the electrode boundaries in $\Re_1$ and that in $\Re_2 \cup \Re_3$ have the opposite sign, which means that $i_1(t)$ is now 180° out-of-phase when compared to $i_2(t)$ and $i_3(t)$. As a result, the previously mentioned combination of the electrode leads causes cancellation around mode 2 excitations. In order to avoid cancellation for excitations around mode 2, one should simply connect the leads coming from $\Re_1$ in the reverse manner (which corresponds to changing the sign of $i_1(t)$). As expected, this modification that we use in order to avoid cancellation for excitations around mode 2 results in cancellation for excitations around mode 1. This discussion is demonstrated in Figure 5(a) and (b), where the voltage and power FRFs (per base acceleration in g) are plotted against a frequency band that includes the first two natural frequencies (and the FRFs are for a fixed resistive load $R_l = 50\,\text{k}\Omega$). The solid line corresponds to the first case that is favorable for mode 1 excitation, but results in cancellation in mode 2 excitations. The dashed line belongs to the case where the cancellation in mode 2 excitation is avoided, but yields cancellation for mode 1 excitation. In practice, it is possible to avoid cancellation

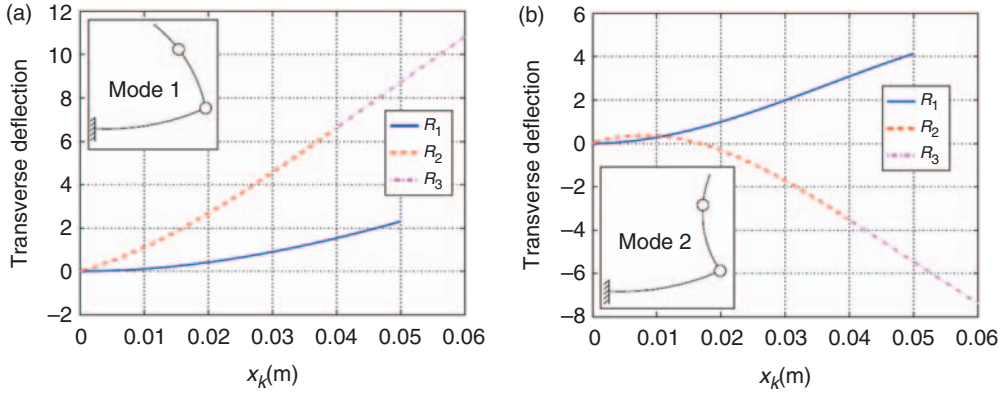

Figure 4. *Mode shapes of the L-shaped piezoelectric energy harvester for the (a) first mode and for (b) the second mode.*

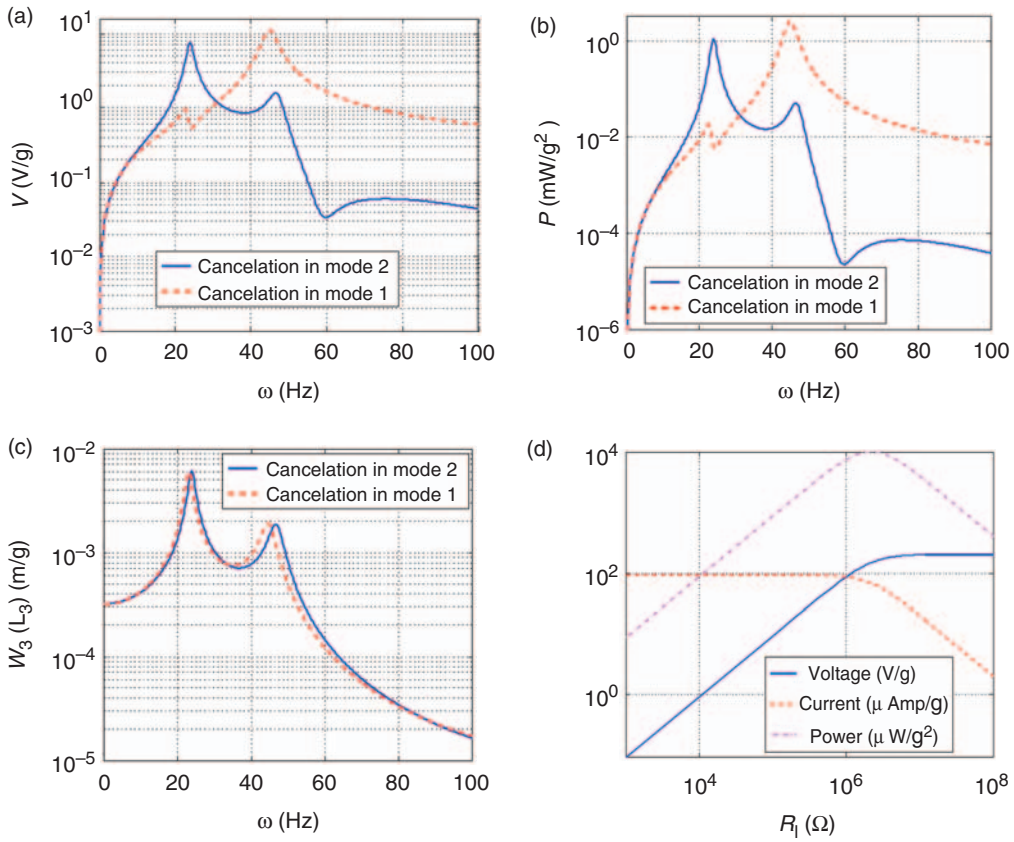

Figure 5. *(a) Voltage, (b) power and (c) tip displacement FRFs for 50 kΩ load resistance, and (d) variation of the voltage, current and power amplitudes with load resistance for the short circuit resonance frequency excitation (at 22.8 Hz).*

of the electrical outputs of $\Re_1$, $\Re_2$, and $\Re_3$ for both vibration modes by employing full-wave rectifiers (Erturk et al., 2008b). It is important to note that the cancellation phenomenon is mainly an electrical issue that depends on the electrode locations, and the major trend in the mechanical FRF is not affected that much. This is depicted in Figure 5(c), which is the FRF that gives the transverse displacement at the free end per base acceleration (in g) for the same resistive load ($R_l = 50\,\text{k}\Omega$). The current FRF can also be obtained from the voltage FRF and it is not shown here. Figure 5(d) shows the variation of the voltage, current and power amplitudes (per base acceleration) for excitation at the short circuit resonance frequency of the first mode ($\omega_1^{sc} \cong 22.8$ Hz). The voltage output increases monotonically whereas the current output decreases monotonically with increasing load resistance. As a consequence of these expected trends in voltage and current, power has a peak value for an optimum resistive load. The largest current output is obtained in short circuit conditions ($R_l \to 0$) as 93 μAmps/g, and the largest voltage output is obtained in open circuit conditions ($R_l \to \infty$) as 203 V/g. An optimum power output of 10 mW/g^2 is extracted for a resistive load of 2.18 MΩ. Note that, similar graphs can be obtained for the second mode excitation (at $\omega_2^{sc} = 45.7$ rad/s) and the optimum load resistance for the excitation at this frequency can be identified. Moreover, a similar analysis can be performed for the open circuit resonance frequencies of the harvester as well.

AN APPLICATION: L-SHAPED ENERGY HARVESTER AS A UAV LANDING GEAR

In this section, first the literature on energy harvesting for UAV applications is reviewed. After discussing a recent work on piezoelectric energy harvesting from landing gears of a UAV (that used uniform cantilever and curved piezoelectric beams), the L-shaped piezoelectric energy harvester configuration is proposed as an improved UAV landing gear. Performance of the L-shaped energy harvester as a UAV landing gear is compared favorably with that of a curved energy harvester beam used for the same purpose in a recent study.

Energy Harvesting for UAVs

UAVs have been investigated by several researchers in the literature (for example Gallington et al., 1996). Moreover, in the last decade, a new class of UAVs, the so-called micro air vehicles (MAVs), has emerged and several research programs were initiated, in particular for use in military-based missions. The main difference between

UAVs and MAVs is due to their dimensional definitions. Although wing spans of typical UAVs can exceed 1 m, the definition of MAVs limits their maximum length dimension to 6 in. (Pines and Bohorquez, 2006). From the practical point of view, our brief discussion in this section applies both for UAVs and MAVs, although, for convenience, we will stick to the term UAV throughout this section. The motivating reasons for harvesting energy in a UAV application include increasing the flight time for a prescribed mission and powering the UAV's sensors or global positioning system units.

The literature includes research on powering UAVs with thermoelectric energy generation (Fleming et al., 2002) as well as detailed discussions on the implementation of solar, wind, electromagnetic, and autophagous (self-consuming) structure-battery applications for UAVs (Qidawi et al., 2005). Piezoelectric energy harvesting for UAVs was discussed by Erturk et al. (2007) and Anton et al. (2008) where AFC (active fiber composite) beams were located inside the fuselage (in the cantilevered configuration) and also attached on the wing spars (as structural patches) of a UAV with a wing span of 1.8 m for voltage generation during the flight. Recently, Magoteaux (2007) studied solar and piezoelectric energy harvesting techniques for implemention in a small UAV. For integrating piezoelectric beams to a UAV, Magoteaux (2007) proposed to replace the landing gears by cantilevered uniform and curved beams as two possible configurations. Even though uniform and curved cantilevered beams are easy to find commercially, these conventional configurations may not be the most appropriate ones to use as landing gears.

Having described the L-shaped piezoelectric energy harvester and its features in this work, we suggest using it as a landing gear for UAV applications where perching is an option for recharging the system. In addition to geometric compatibility of the L-shaped structure as a landing gear (Figure 6), its parameters can be tuned to obtain the two-to-one internal resonance to a prescribed primary resonance, as discussed previously. Reasonably, one should be careful with the size and weight limitations of the UAV while designing the L-shaped energy harvester. The primary resonance of interest is the dominant excitation frequency and it might be the operating frequency of a vibrating base on which the UAV lands during a mission, as depicted in Figure 6. As a concrete example, one can consider an MAV, which lands on a vibrating air conditioner unit during the mission to charge its batteries. Typical frequency contents of such devices have been provided in the literature on energy harvesting (Roundy et al., 2003); hence, one can select a dominant primary resonance to obtain the best electrical results in piezoelectric energy harvesting. Considering Figure 6, it is worthwhile to add that the L-shaped energy harvester as a landing gear

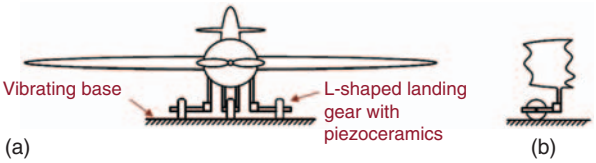

Figure 6. *Schematic of a UAV with L-shaped – energy harvester – landing gears; (a) front view of the UAV and (b) side view of the front landing gear.*

has somewhat different boundary conditions and mechanical forcing when compared to what has been investigated in this work based on Figure 2(a). One can easily modify the boundary conditions given by Equations (3a)–(3h), as well as the mechanical forcing term, to represent the excitation coming from the wheels. Note that the wheel of each landing gear can take the place of the second lumped mass between segments $\Re_2$ and $\Re_3$. Alternatively, the given formulation can be used directly by equating the length of $\Re_3$ to zero and the partial lumped mass of the UAV to M_2 (Figure 2(a)). Then, the clamped end is the location of the wheel with the ground acceleration $a_B(t)$. The mass of the UAV can be split and lumped on each landing gear to analyze the electrical outputs for a given vibratory motion at each wheel. This option is also in agreement with the approach used in the aforementioned work (Magoteaux, 2007). Therefore, the following analysis considers the split-mass of the UAV as M_2 and the base acceleration as the vertical acceleration at the wheel.

A Comparative Case Study

As mentioned before, Magoteaux (2007) studied two types of harvesters in his landing gear application for a small UAV: a curved beam and a uniform cantilevered beam. The total mass of the UAV (150 g) was split into two or three lumped masses (for two or three landing gears, respectively) to estimate the electrical power outputs of the curved and the uniform harvester beam alternatives. Hence, one case was for 75 g tip mass per landing gear whereas the other case was for 50 g tip mass per landing gear (theoretically, the case of 25 g tip mass per landing gear was studied as well, which should correspond to the case of having six beams, and which may not be as practical). Relying on the mathematical model (due to its predictions for the case without the UAV mass), Magoteaux (2007) examined the uniform beam case theoretically, whereas he investigated the curved beam case with the UAV mass experimentally. After comparing the model predictions for the uniform beam case with the experimental results of the curved beam case, Magoteaux (2007) concluded that the uniform cantilevered beam case yields higher outputs at relatively low frequencies. This statement could be misleading, as the displacement response of the harvester was not checked in the theoretical study. For the uniform cantilevered beam case, a tip mass of

50 g (due to 1/3 of the UAV mass) is about 137 times the mass of each harvester beam (i.e., each landing gear), whereas a tip mass of 75 g (due to 1/2 of the UAV mass) is about 206 times the mass of each harvester beam. It can be shown by using the analytical solution for a cantilevered beam (Erturk and Inman, 2008a) that, even for impractically large mechanical damping ratios, both of these cases result in very large displacement response amplitudes at resonance when compared to the dimensions of the uniform harvester beam (Table 4.2 in Magoteaux (2007)) for the given acceleration input ($10\,\mathrm{m/s^2}$). Therefore, the theoretical predictions of the uniform harvester model fail for the aforementioned numerical values (most likely, in practice, a real harvester described by these numerical data would also fail under large deflections). Hence, for an approximate comparison, we consider the experimental results of the curved beam configuration in Magoteaux (2007) and focus on the case with a 50 g tip mass due to 1/3 of the UAV mass, which is an estimate of using 3 landing gears.

The curved harvester beam used by Magoteaux (2007) was a THUNDER Actuator TH-8R supplied by the Face® International Corporation. The length, width, and total thickness of this curved beam are 63.25 mm, 13.72 mm, and 0.43 mm. The substrate of the curved beam is stainless steel (Face®, 2008). For the case with a tip mass of 50 g and an acceleration input of $10\,\mathrm{m/s^2}$ (realized through a shaker), Magoteaux (2007) obtained a maximum power output of about 1.1 mW with a voltage output of about 7 v. Hence, one can extract the optimum resistive load that yields the maximum power output approximately as 44 kΩ. Next, an L-shaped – energy harvester – landing gear is designed as an alternative to the curved beam used in the mentioned work.

For accurate modeling of the L-shaped energy harvester as a landing gear, one can modify the boundary conditions of the structure (Figure 2(a)) described previously. However, it is also possible to model the landing gear structure without changing the formulation given in this article and this is what we prefer here. If the length of the harvester segment $\Re_3$ equals zero ($L_3 = 0$) in Figure 2(a), the harvester structure consists of segments $\Re_1$ and $\Re_2$ only. One can then consider the lumped mass M_2 as the split mass of the UAV on each landing gear ($M_2 = 50$ g). As mentioned in the distributed parameter formulation, the split weight $M_2 g$ of the UAV acts as an axial load for segment $\Re_2$. Furthermore, a rotary inertia (J_2) can be specified for the UAV about the respective axis at the point of connection between the UAV and the landing gear. As can be anticipated, the clamped end in $\Re_1$ is the location of the wheel where the ground acceleration input is known ($A_B = 10\,\mathrm{m/s^2}$). Since the acceleration input at the wheel is known, the mass of the wheel is redundant. It is important to note that the given formulation restricts the slope at the wheel to be zero.[3] In addition to the UAV mass described by M_2, the formulation allows another mass at the corner of the harvester (M_1 with the rotary inertia J_1). Here, M_1 might be a useful parameter in order to tune the natural frequencies of the landing gear, or, practically, it might represent the mass of a stiffener at the corner (for simplicity, it can be taken as zero).

Table 3. Geometric properties of the L-shaped – energy harvester – landing gear.

Segment	Dimension	Substructure	Piezoceramic
$\Re_1$	Length (mm)	30	30
	Width (mm)	10	10
	Thickness (mm)	0.3	0.3
$\Re_2$	Length (mm)	20	20
	Width (mm)	10	10
	Thickness (mm)	0.2	0.2

Here, the attention is given to keeping the total length of the L-shaped energy harvester, its thickness, and width similar to those of the curved harvester used by Magoteaux (2007). The geometric data of the L-shaped – energy harvester – landing gear is displayed in Table 3 and its material properties are given in Table 1. Hence, the materials of piezoceramic and substructure are PZT-5A and stainless steel, respectively. In addition, $M_2 = 50$ g, $M_1 = J_1 = J_2 = 0$ and the harvester consists of segments M_1 and M_2 only, since $L_3 = 0$. For a more accurate analysis, the rotary inertia J_2 of the UAV can be included in the calculations. Note that, with these data, the L-shaped structure has a total mass of 1.95 g (excluding the wheel and the UAV mass) and it is slightly less than the mass of the THUNDER Actuator TH-8R used by Magoteaux (2007), which is 2.1 g (Face®, 2008). Thus, the comparison basis is fair in terms of the amount of the mass added to the UAV as a landing gear. Instead of presenting the electrical outputs at resonance as done by Magoteaux (2007), we present the results with FRFs as done in the case study. For a resistive load of $R_l = 44\,\mathrm{k\Omega}$ (which is approximately the optimum resistive load of the configuration in Magoteaux (2007)), the voltage FRF (per g) is shown in Figure 7(a). Note that $R_l = 44\,\mathrm{k\Omega}$, however, is not the optimum resistive load of the harvester presented here. The issue regarding the combination of the electrode leads of segments $\Re_1$ and $\Re_2$ generators persists (see the discussion in the case study) and one can combine these leads to avoid cancellations for mode 1 or mode 2 excitations, separately. The first two resonance frequencies of the harvester in short circuit conditions ($R_l \to 0$) are 16.4 Hz and 49.3 Hz, respectively. These two frequencies, respectively, shift to the open circuit resonance frequencies 17.0 Hz and 49.7 Hz,

[3]Although base rotation is not discussed in this work, one might as well specify a small rotation at the base, as described by Erturk and Inman (2008a) for the unimorph cantilevered energy harvester case. Inclusion of base rotation results in a modification of the modal forcing function given by Equation (9b).

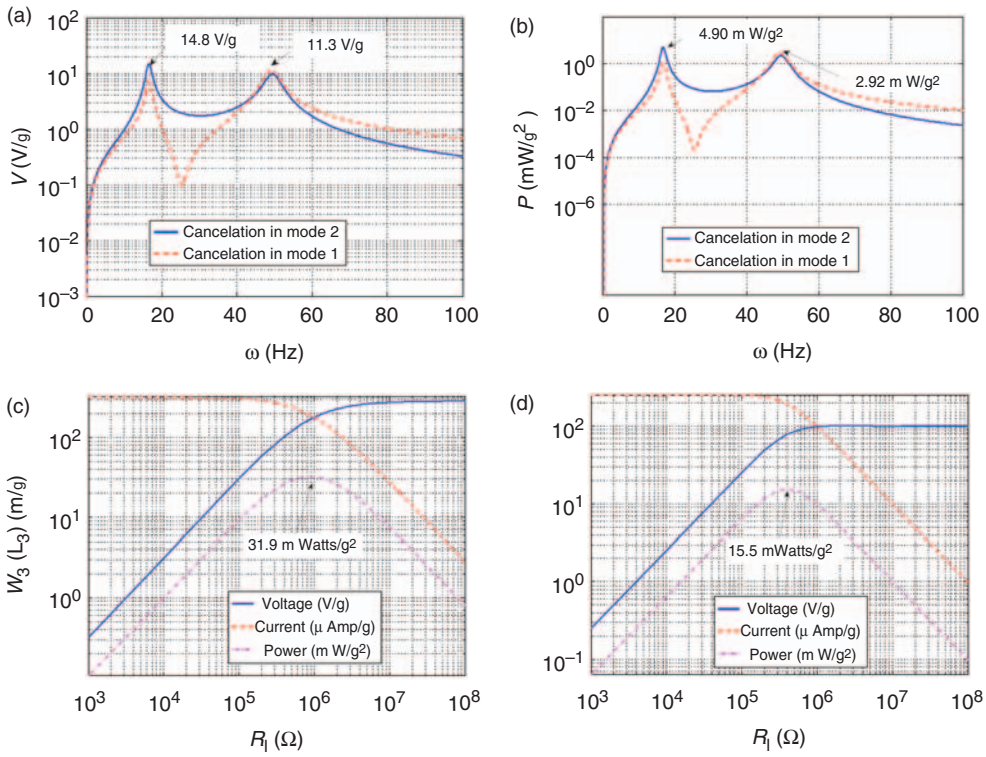

Figure 7. *(a) Voltage and (b) power FRFs for a 44 kΩ load resistance and variation of the voltage, current, and power amplitudes with load resistance for the short circuit resonance frequency excitation of the (c) first mode (at 16.4 Hz) and the (d) second mode (at 49.3 Hz).*

as $R_l \to \infty$. It can be seen from the voltage FRF for $R_l = 44\text{k}\Omega$ that the maximum voltage amplitude can be as high as 14.8 V/g, and 11.3 V/g for mode 1 and mode 2 excitations, respectively. The electrical power FRF is shown in Figure 7(b) for the same resistive load, and the maximum power for mode 1 and mode 2 excitations can be read from the graph as 4.90 mW/g^2 and 2.92 mW/g^2, respectively. The transverse deflection amplitudes at the critical points ($x_1 = L_1$ and $x_2 = L_2$) are found to be < 3 mm/g and 4 mm/g, respectively, for 4% modal mechanical damping. Figure 7(c) and (d) display the variation of voltage, current and power amplitudes with load resistance for mode 1 and mode 2 excitations, at $\omega_1^{sc} = 16.4$ Hz and at $\omega_2^{sc} = 49.3$ Hz, respectively. In Figure 7(c), the leads of the electrodes coming from segments $\Re_1$ and $\Re_2$ are combined to avoid cancellation for mode 1 excitation, whereas, in Figure 7(d), the leads are combined to avoid cancellation for mode 2 excitation. The maximum voltage and current amplitudes in Figure 7(c) are 281.8 V/g (for open circuit conditions, $R_l \to \infty$) and 316 μAmps/g (for short circuit conditions, $R_l \to 0$), respectively. The maximum power amplitude in Figure 7(c) is about 31.9 mW/g^2 for an optimum resistive load of 870 kΩ. One can read the maximum voltage and current amplitudes in Figure 7(d) as 100 V/g (for open circuit conditions) and 251 μAmps/g (for short circuit conditions), respectively. The maximum power amplitude in Figure 7(d) is about 15.5 mW/g^2 for an optimum resistive load of 398 kΩ.

It is clear from Figure 7(c) and (d) that the optimum load resistance of the L-shaped energy harvester is relatively large (in the order of hundreds of kΩ) and the maximum power obtained for the optimum resistive load is also much larger when compared to the curved harvester beam case. Magoteaux (2007) was able to extract 1.1 mW from the curved harvester (THUNDER Actuator TH-8R) for a harmonic ground acceleration with amplitude of 10 m/s^2 (slightly higher than 1 g) and at a resonance frequency of 145 Hz (for the optimum resistive load of 44 kΩ). Here, for the same resistive load (44 kΩ) and 1 g acceleration input, the L-shaped – energy harvester – landing gear gives 4.9 mW at 16.4 Hz and 2.92 mW at 49.3 Hz (Figure 7(b)). Although 44 kΩ is not the optimum resistive load for the L-shaped energy harvester used here, the power outputs obtained at these two resonance frequencies are still larger than the maximum power (1.1 mW) obtained from the curved harvester used by Magoteaux (2007). Since the optimum load resistance of the L-shaped configuration is relatively large, the electrical power increases monotonically as one increases the resistive load from low values to a certain value in the order of hundreds of kΩ (Figure 7(c) and (d) for mode 1 and mode 2 excitations, respectively). Based on these promising results of the model proposed, the authors are currently investigating the experimental performance of the L-shaped beam-mass structure as a piezoelectric energy harvester.

SUMMARY AND CONCLUSIONS

In this work, an L-shaped beam-mass structure is proposed as a novel piezoelectric energy harvester configuration with the capability of producing a broader band harvesting system. A distributed parameter model is proposed to analyze the coupled electromechanical behavior of the L-shaped piezoelectric energy harvester and a direct application is proposed for UAVs. The L-shaped structure can be tuned to have the first two natural frequencies much closer to each other (on the frequency axis) when compared to the conventional cantilevered beam case. Reasonably, having the first two natural frequencies close to each other is a favorable feature in the sense of broadband energy harvesting for random or varying-frequency excitations.

An electromechanical model is presented for a detailed analysis, where the L-shaped piezoelectric energy harvester is investigated as a generator with three thin beam segments. The coupled model is developed based on a recent distributed parameter piezoelectric energy harvester formulation. The electrical outputs of the three piezoceramic segments are combined in series and connected to a resistive electrical load. The frequency response functions of the voltage across the resistive load, and electrical power as well as the coupled mechanical response of the harvester are investigated (per base acceleration). Variations of the voltage, current, and power amplitudes with load resistance are also examined and the well-known qualitative trends are observed (such as the existence of an optimum resistive load for the maximum electrical power and the short circuit and open circuit resonance frequencies). In addition, how to combine the electrodes of the piezoelectric layers is discussed to avoid the possible mode shape dependent voltage cancellations.

Finally, a direct application is discussed where the L-shaped energy harvesters are suggested for use as UAV landing gears. Improving the flight time of UAVs during the mission and powering their sensors and global positioning units is an important research topic. Here, the L-shaped energy harvester configuration is proposed as a UAV landing gear for harvesting electrical energy from perching during the mission. A case study is presented to compare the L-shaped – energy harvester – landing gear with a curved energy harvester beam that was used for the same purpose in a recent work. The significant advantage of using the L-shaped energy harvester (having the same mass and resistive load as that of the curved beam harvester) is demonstrated theoretically. Based on the promising theoretical results of this novel piezoelectric energy harvester configuration, the authors are currently investigating the experimental performance of the L-shaped beam-mass structure for piezoelectric energy harvesting.

APPENDIX

Mass per unit length of segment $\Re_k$ can be given by:

$$m_k = b_k\left[(\rho_s)_k(h_s)_k + (\rho_p)_k(h_p)_k\right], \tag{21}$$

where $(\rho_s)_k$ and $(\rho_p)_k$ are mass densities of the substructure and piezoceramic layers, respectively. The thicknesses are given by $(h_s)_k$ and $(h_p)_k$ for the substructure and the piezoceramic layers, respectively, and both layers are assumed to have the same width b_k in segment $\Re_k$ (Figure 8).

The bending stiffness of the composite cross-section can be expressed as:

$$YI_k = \frac{b_k}{3}\left[(Y_s)_k\left((h_b)_k^3 - (h_a)_k^3\right) + (Y_p)_k\left((h_c)_k^3 - (h_b)_k^3\right)\right], \tag{22}$$

where $(Ys)_k$ and $(Y_p)_k$ are the Young's moduli of the substructure and the piezoceramic layers, respectively. Note that $(Y_p)_k$ is indeed the elastic stiffness of the piezoceramic at constant electric field, i.e., $(Y_p)_k = \left(c_{11}^E\right)_k$. Furthermore, $(h_a)_k$ is the position of the bottom of the substructure layer from the neutral axis (always negative), $(h_b)_k$ is the position of the top of the substructure layer from the neutral axis (positive or negative), and $(h_c)_k$ is the position of the top of the piezoceramic layer from the neutral axis (always positive):

$$\begin{aligned}
(h_a)_k &= -\frac{(h_p)_k^2 + 2(h_p)_k(h_s)_k + n_k(h_s)_k^2}{2\left[(h_p)_k + n_k(h_s)_k\right]},\\
(h_b)_k &= \frac{n_k(h_s)_k^2 - (h_p)_k^2}{2\left[(h_p)_k + n_k(h_s)_k\right]},\\
(h_c)_k &= \frac{(h_p)_k^2 + 2n_k(h_p)_k(h_s)_k + n_k(h_s)_k^2}{2\left[(h_p)_k + n_k(h_s)_k\right]},
\end{aligned} \tag{23}$$

where $n_k = (Y_s)_k/(Y_p)_k$ is the Young's moduli ratio.

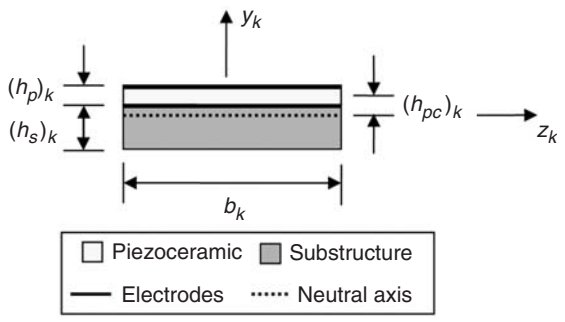

Figure 8. *Cross-sectional view of the k-th unimorph segment.*

The distance from the center of the piezoceramic layer to the neutral axis in segment $\Re_k$ can be expressed as:

$$(h_{pc})_k = \frac{n_k(h_s)_k\left[(h_p)_k + (h_s)_k\right]}{2\left[(h_p)_k + n_k(h_s)_k\right]}. \quad (24)$$

Finally, the electromechanical coupling coefficient in the physical coordinates for segment $\Re_k$ of the structure can be given by:

$$\vartheta_k = \frac{(Y_p)_k(\mathrm{d}_{31})_k b_k}{2(h_p)_k}\left[(h_b)_k^2 - (h_c)_k^2\right], \quad (25)$$

where $(\mathrm{d}_{31})_k$ is the piezoelectric constant of the piezoceramic layer in $\Re_k$.

ACKNOWLEDGMENTS

The authors gratefully acknowledge the support of the Air Force Office of Scientific Research (AFOSR) MURI under grant number F 9550-06-1-0326 'Energy Harvesting and Storage Systems for Future Air Force Vehicles' monitored by Dr B.L. Lee. The authors also thank Dr Brian Sanders of the Air Force Research Laboratory (AFRL) for helpful discussions on the UAV landing gear concept.

REFERENCES

Anton, S.R. and Sodano, H.A. 2007. "A Review of Power Harvesting using Piezoelectric Materials (2003)–(2006)," *Smart Materials and Structures*, 16:R1–R21.

Anton, S.R., Erturk, A. and Inman, D.J. 2008. "Energy Harvesting from Small Unmanned Air Vehicles," In: *Proceedings of the 17th International Symposium on Application of Ferroelectrics, 3rd Annual Energy Harvesting Workshop*, 24–27 February 2007, Santa Fe, NM.

Arnold, D.P. 2007. "Review of Microscale Magnetic Power Generation," *IEEE Transactions on Magnetics*, 43:3940–3951.

Baker, J.M., Roundy, S. and Wright, P.K. 2005. "Alternative Geometries for Increasing Power Density in Vibration Energy Scavenging for Wireless Sensor Networks," In: *Proceedings of 3rd International Energy Conversion Engineering Conference*, 15–18 August 2005, San Francisco, CA.

Balachandran, B. and Nayfeh, A.H. 1990. "Nonlinear Motions of Beam-mass Structure," *Nonlinear Dynamics*, 1:39–61.

Beeby, S.P., Tudor, M.J. and White, N.M. 2006. "Energy Harvesting Vibration Sources for Microsystems Applications," *Measurement Science and Technology*, 17:175–195.

Chopra, A. 2007. *Dynamics of Structures: Theory and Applications to Earthquake Engineering*, Prentice Hall, New Jersey.

Cook-Chennault, K.A., Thambi, N. and Sastry, A.M. 2008. "Powering MEMS Portable Devices – A Review of Non-regenerative and Regenerative Power Supply Systems with Emphasis on Piezoelectric Energy Harvesting Systems," *Smart Materials and Structures*, 17:043001:1–33.

duToit, N.E., Wardle, B.L. and Kim, S.G. 2005. "Design Considerations for MEMS-scale Piezoelectric Mechanical Vibration Energy Harvesters," *Journal of Integrated Ferroelectrics*, 71:121–160.

Erturk, A., Anton, S.R. and Inman, D.J. 2007. "Energy Harvesting from Rigid Body Motions," In: *Proceedings of the 18th International Conference of Adaptive Structures and Technologies*, 3–5 October 2007, Ottawa, Ontario, Canada.

Erturk, A. and Inman, D.J. 2008a. "A Distributed Parameter Electromechanical Model for Cantilevered Piezoelectric Energy Harvesters," *ASME Journal of Vibration and Acoustics*, 130:041002:1–15.

Erturk, A., Tarazaga, P.A., Farmer, J.R. and Inman, D.J. 2008b. "Effect of Strain Nodes and Electrode Configuration on Piezoelectric Energy Harvesting from Cantilevered Beams," *ASME Journal of Vibration and Acoustics*, 10.1115/1.2981094.

Erturk, A. and Inman, D.J. 2008c. "An Experimentally Validated Bimorph Cantilever Model for Piezoelectric Energy Harvesting from Base Excitations," *Smart Materials and Structures* (in review).

Erturk, A. and Inman, D.J. 2008d. "On Mechanical Modeling of Cantilevered Piezoelectric Vibration Energy Harvesters," *Journal of Intelligent Material Systems and Structures*, 19, 10.1177/1045389X07085639 (in press).

Face® 2008. TH-8R data sheet. URL http://www.faceco.com

Fleming, J., Ng, W. and Ghamaty, S. 2002. "Thermoelectric-based Power System for UAV/MAV Applications," *Proceedings of 1st Technical Conference and Workshop in Unmanned Aerospace Vehicles*, 20–23 May 2002, Portsmouth, VA.

Gallington, R.W., Merman, H., Entzminger, J., Francis, M.S., Palmore, P. and Stratakes, J. 1996. "Unmanned Aerial Vehicles," *Future Aeronautical and Space Systems*, AIAA, 172:251–296.

Guyan, R. 1965. "Reduction of Stiffness and Mass Matrices," *AIAA Journal*, 3:380.

Haddow, A.G., Barr, A.D.S. and Mook, D.T. 1984. "Theoretical and Experimental Study of Modal Interaction in a Two-degree-of-freedom Structure," *Journal of Sound and Vibration*, 97:451–473.

Hu, Y., Xue, H. and Hu, H. 2007. "A Piezoelectric Power Harvester with Adjustable Frequency through Axial Preloads," *Smart Materials and Structures*, 16:1961–1966.

Lesieutre, G.A., Ottman, G.K. and Hofmann, H.F. 2004. "Damping as a Result of Piezoelectric Energy Harvesting," *Journal of Sound and Vibration*, 269:991–1001.

Magoteaux, K. 2007. Investigation of an Energy Harvesting Small Unmanned Air Vehicle. Master of Science Thesis, University of Dayton.

Mitcheson, P.D., Miao, P., Start, B.H., Yeatman, E.M., Holmes, A.S. and Green, T.C. 2004. "MEMS Electrostatic Micro-Power Generator for Low Frequency Operation," *Sensors and Actuators A*, 115:523–529.

Nayfeh, A.H. and Mook, D.T. 1979. *Nonlinear Oscillations*, Wiley, New York.

Ottman, G.K., Hofmann, H.F., Bhatt, A.C. and Lesieutre, G.A. 2002. "Adaptive Piezoelectric Energy Harvesting Circuit for Wireless Remote Power Supply," *IEEE Transactions on Power Electronics*, 17:669–676.

Oueini, S.S., Nayfeh, A.H. and Pratt, J.R. 1998. "A Nonlinear Vibration Absorber for Flexible Structures," *Nonlinear Dynamics*, 15:259–282.

Pines, D.J. and Bohorquez, F. 2006. "Challenges Facing Future Micro-air-vehicle Development," *AIAA Journal of Aircraft*, 43:290–305.

Priya, S. 2007. "Advances in Energy Harvesting using Low Profile Piezoelectric Transducers," *Journal of Electroceramics*, 19:167–184.

Qidawi, M.A., Thomas, J.P. and Kellogg, J.C. 2005. "Expanding Mission Capabilities of Unmanned Systems through the

Collection of Energy in the Field,'' In: *Proceedings of the AIAA 3rd International Energy Conversion Engineering Conference*, 15–18 August 2008, San Francisco, CA.

Rao, S.S. 2007. *Vibration of Continuous Systems*, Wiley, New York.

Roundy, S.,Wright, P.K. and Rabaey, J. 2003. ''A Study of Low Level Vibrations as a Power Source for Wireless Sensor Nodes,'' *Computer Communications*, 26:1131–1144.

Sodano, H.A., Park, G. and Inman, D.J. 2004. ''Estimation of Electric Charge Output for Piezoelectric Energy Harvesting.'' *Strain*, 40:49–58.

Sodano, H.A., Inman, D.J. and Park, G. 2005. ''Generation and Storage of Electricity from Power Harvesting Devices,'' *Journal of Intelligent Material Systems and Structures*, 16:67–75.

Williams, C.B. and Yates, R.B. 1996. ''Analysis of a Micro-electric Generator for Microsystems,'' *Sensors and Actuators A*, 52:8–11.